# A unified framework to identify demographic buffering in natural populations

Gabriel Santos[1], Samuel Gascoigne[2], André Dias[3], Maja Kajin[2], and Roberto Salguero-Gomez[2]

[1]National Institute of the Atlantic Forest (INMA)
[2]University of Oxford
[3]Universidade Federal do Rio de Janeiro

July 19, 2023

**Abstract**

The Demographic Buffering Hypothesis (DBH) predicts that natural selection reduces the temporal fluctuations in demographic processes (such as survival, development, and reproduction), due to their negative impacts on population dynamics. However, a comprehensive approach that allows for the examination of demographic buffering patterns across multiple species is still lacking. Here, we propose a three-step framework aimed at identifying and quantifying demographic buffering. Firstly, we categorize species along a continuum of variance based on their stochastic elasticities. Secondly, we examine the linear selection gradients, followed by the examination of nonlinear selection gradients as the third step. With these three steps, our framework overcomes existing limitations of conventional approaches to identify and quantify demographic buffering, allows for multi-species comparisons, and offers insight into the evolutionary forces that shape demographic buffering. We apply this framework to mammal species and discuss both the advantages and potential of our framework.

**A unified framework to identify demographic buffering in natural populations**

A manuscript in preparation for submission to ECOLOGY LETTERS

Type of article: METHOD

Gabriel Silva Santos [1,2*], Samuel J L Gascoigne[3*], André Tavares Corrêa Dias[4], Maja Kajin [3,5**♦], Roberto Salguero-Gómez[3♦]

1 National Institute of the Atlantic Forest (INMA), 29650-000, Santa Teresa, Espirito Santo, Brazil. ssantos.gabriel@gmail.com

2 Department of Ecology, Graduate Program in Ecology and Evolution, Rio de Janeiro State University, 524 São Francisco Xavier street, 20550-900, Maracanã, Rio de Janeiro, Brazil

3 Department of Biology, University of Oxford, South Parks Road, OX1 3RB, Oxford, UK. samuel.gascoigne@pmb.ox.ac.uk, rob.salguero@biology.ox.ac.uk, maja.kajin@biology.ox.ac.uk

4 Department of Ecology, Institute of Biology, Universidade Federal do Rio de Janeiro, Avenida Carlos Chagas Filho 373, 21941-590 Rio de Janeiro, RJ, Brazil. atcdias@gmail.com

5 Department of Biology, Biotechnical Faculty, University of Ljubljana, Večna pot 111, 1000 Ljubljana, Slovenia

*Shared first authorship

**Corresponding author

♦Shared senior authorship

AUTHOR CONTRIBUTIONS: GSS developed the initial concept, performed the statistical analyses and contributed to the first draft of the manuscript. SJLG developed the initial concept, contributed to the first draft and all other versions of the manuscript and generated final figures. ATCD co-advised the project and contributed significantly to final versions of the manuscript. MK developed and managed the project, contributed to the first draft and all other versions of the manuscript and generated final figures. RSG developed and managed the project and contributed to the first draft and all other versions of the manuscript. All authors made substantial contributions to editing the manuscript and further refining ideas and interpretations.

RUNNING TITLE: Demographic buffering framework (31/45 words)

KEYWORDS: COMADRE Animal Matrix Database, elasticity, life-history evolution, natural selection, second-order derivative, sensitivity, stochasticity, variance.

NUMBER OF WORDS: Abstract – 146/150 words, main text (excluding abstract, acknowledgements, references, table and figure legends) – 5398/5000 words

NUMBER OF REFERENCES: 64

NUMBER OF TABLES: 1 (in Supplementary Material)

NUMBER OF FIGURES: 3

**Abstract** (146/150 words)

The Demographic Buffering Hypothesis (DBH) predicts that natural selection reduces the temporal fluctuations in demographic processes (such as survival, development, and reproduction), due to their negative impacts on population dynamics. However, a comprehensive approach that allows for the examination of demographic buffering patterns across multiple species is still lacking. Here, we propose a three-step framework aimed at identifying and quantifying demographic buffering. Firstly, we categorize species along a continuum of variance based on their stochastic elasticities. Secondly, we examine the linear selection gradients, followed by the examination of nonlinear selection gradients as the third step. With these three steps, our framework overcomes existing limitations of conventional approaches to identify and quantify demographic buffering, allows for multi-species comparisons, and offers insight into the evolutionary forces that shape demographic buffering. We apply this framework to mammal species and discuss both the advantages and potential of our framework.

Environmental stochasticity plays a pivotal role in shaping organisms' life histories (Bonsall & Klug 2011). Nonetheless, how organisms will cope with the increasing variation in environmental conditions expected under climate change (Boyce *et al.* 2006; Morris *et al.* 2008) is one of the most intriguing questions of ecology and evolution (Sutherland *et al.* 2013). Evolutionary demography offers a wide array of explanations for the evolutionary processes that shape the diversity of demographic responses to environmental stochasticity (Charlesworth 1994; Pfister 1998; Tuljapurkar *et al.* 2009; Healy *et al.* 2019; Hilde *et al.* 2020). The Demographic Buffering Hypothesis (*DBH*, hereafter) (Morris & Doak 2004; Pélabon *et al.* 2020) predicts a negative relationship between the contribution of a demographic processes (*e.g.*, survival, development, reproduction) to the population growth rate ($\lambda$) and their temporal variance (Pfister 1998). The emerging demographic strategy, demographic buffering, accommodates variance of demographic processes to cope with the otherwise negative effects of stochastic environments on $\lambda$ (Pfister 1998; Morris & Doak 2004; Hilde *et al.* 2020).

A unified approach to unambiguously quantify demographic buffering is still missing. Indeed, identifying demographic buffering remains challenging (Morris & Doak 2004; Doak *et al.* 2005) for at least three reasons. First is the different interpretation of results from correlational analyses (*e.g.*, as in Pfister, 1998). Some authors have used the correlation coefficient as an index to order species' life histories in a continuum ranging from buffered (Spearman's correlation $\rho = <0$ between the sensitivity of $\lambda$ to demographic processes and their temporal variance) to labile ($\rho = >0$, regardless of the "scatterness" around the regression (McDonald *et al.* 2017). In contrast, other researchers interpret the absence of statistical support for demographic buffering as an alternative strategy where variance in demographic process(es) is favoured to track environmental conditions (the so-called Demographic Lability Hypothesis (*DLH*, hereafter; *e.g.,*(Koons *et al.* 2009; Reed & Slade 2012; Jäkäläniemi *et al.* 2013; Hilde *et al.* 2020).

92 The second obstacle to obtain generalisation across species' populations regarding
93 demographic buffering is the hierarchical level at which this phenomenon is typically
94 examined. Some studies base their investigations of demographic buffering on the *whole* life
95 history at the level of species or populations (*interspecific level*, hereafter), focusing on the
96 one demographic process that is the most influential for $\lambda$ (Reed & Slade 2012; McDonald *et al.*
97 2017). At the interspecific level, a life history is referred to as demographically buffered if the
98 most important demographic process has low temporal variance (Pfister 1998; Morris & Doak
99 2004; Hilde *et al.* 2020; Le Coeur *et al.* 2022). Thus, the associated strategy is commonly
100 decided based on a *single* demographic process (*e.g.*, adult survival), ignoring the selection
101 pressures on the rest of the demographic processes within the life cycle. However, to
102 understand how, why, and where demographic buffering occurs –or not– and how buffering
103 patterns might be modified in response to the environment, it is essential to also consider the
104 features *within* a single species' life cycle (*intraspecific level*, hereafter). Within a single life
105 cycle one demographic process can be buffered against while another can be labile to the
106 environment – supporting the DLH (Koons *et al.* 2009; Jongejans *et al.* 2010; Barraquand &
107 Yoccoz 2013). Thus, for a mechanistic understanding of how environmental stochasticity
108 shapes life histories, both inter- and intra-specific levels need to be addressed.
109 The third reason limiting a holistic understanding of demographic strategies in
110 stochastic environments are the challenges inherent to examining their underlying
111 mechanisms. Evidence for demographic buffering exists across some long-lived organisms
112 with complex life cycles, (Pfister 1998; Gaillard & Yoccoz 2003; Doak *et al.* 2005; Rotella *et al.*
113 2012; McDonald *et al.* 2017), but also in short-lived species (Pfister 1998; Reed & Slade 2012;
114 Ferreira *et al.* 2013). Importantly, these patterns of variation do not inform on how the life
115 histories were shaped by natural selection. To do so, one would need to identify the type
116 (linear or nonlinear) and strength of selection acting on demographic processes. Linear

117 selection acts on changing *the mean* value of a demographic process via a linear function
118 between the fitness and the demographic process. In contrast, nonlinear selection acts on *the*
119 *variance* of demographic processes either increasing it, decreasing it, or
120 increasing/decreasing *the covariance* between two demographic processes (Brodie et al.
121 1995; Carslake et al. 2008).

122 The sign of the self-second derivative of $\lambda$ determines the type of nonlinear selection
123 acting on a demographic process. For instance, a negative self-second derivative for a given
124 demographic process describes a concave form of selection, commonly referred to as the ∩-
125 shaped selection (Caswell 1996, 2001; Shyu & Caswell 2014). This form of selection reduces the
126 temporal variance in said demographic process, thereby providing support for the DBH.
127 Conversely, a demographic process yielding a positive self-second derivative identifies a
128 convex, or U-shaped selection (Caswell 1996, 2001; Shyu & Caswell 2014). Such a selection
129 mechanism acts upon demographic processes amplifying their temporal variance, thus
130 supporting the DLH (Koons *et al.* 2009; Le Coeur *et al.* 2022). The cross-second derivatives (not
131 discussed here, see Caswell 1996, 2001 for further details) quantify selection pressures acting
132 on the strength of correlation among different demographic processes.

133 The rich variation in demographic strategies across the Tree of Life is a result of
134 evolutionary processes that have shaped variance in demographic processes through time. In
135 this context, setting demographic buffering into the adaptive landscape context of linear and
136 nonlinear selection enables us to identify and quantify the evolutionary processes that
137 generate said demographic patterns. In this way, one will better understand how increased
138 variability of environmental conditions might act on the existing –and shape novel–
139 demographic strategies. However, we still lack a unified approach to quantify DBH.

140 Here, we present a framework that identifies and quantifies demographic buffering.
141 Our framework provides a thorough analysis of temporal variance in demographic processes

142 affected by environmental stochasticity. This framework involves categorizing species or
143 populations along a variance continuum based on the extent to which key demographic
144 processes are buffered by natural selection, thereby limiting their temporal variability. The
145 framework consists of four steps with a mix of well-known methods applied to stage-
146 structured demographic information (*e.g.,* matrix population models [Caswell 2001]; integral
147 projection models [Easterling et al. 2000]). First, we position species or populations on the
148 aforementioned continuum to assess the cumulative effect of the variance on their key
149 demographic processes at the interspecific level (see below). Second, we investigate the
150 presence of linear selection forces operating within the life cycle of each species or
151 population at the intraspecific level (below). Third, we explore the impact of non-linear
152 selection forces acting within the life cycle of each species or population, also at the
153 intraspecific level. The combination of these three steps provides quantitative evidence
154 for/against the DBH, while in step four we describe how to test the DLH.
155 To demonstrate the applicability of our framework, we apply it to 40 populations of
156 34 mammal species sourced from the COMADRE database (Salguero-Gómez *et al.* 2016). We
157 showcase how the framework can provide valuable insights into the patterns of demographic
158 buffering across species. The framework offers novel, detailed insights into the selection
159 pressures that act *within* species' life cycles, thus allowing for a thorough understanding of
160 the evolutionary selection forces that shape the patterns of demographic buffering across
161 species. Beyond providing a quantitative, systematic toolset to test the DBH through three
162 steps, we have also offer an alternative fourth step that briefly outlines how to test for the
163 DLH.
164

**A unified framework to assess evidence of DBH**

The evidence for demographic buffering has been mainly assessed using Matrix Population Models (Pfister 1998; Rotella *et al.* 2012). However, Integral Projection Models (IPM; Rodríguez-Caro et al. 2020; Wang et al. 2023) can be equally applied for identifying the demographic buffering signatures. Both MPMs and IPMs are stage-structured, discrete-time demographic models (Caswell 2001; Ellner *et al.* 2016). For simplicity, here we focus on MPMs, but note that the same approaches are as equally applicable to IPMs (Griffith 2017; Doak *et al.* 2021). Throughout this manuscript, we refer to demographic processes as both matrix entries $a_{ij}$ (*i.e.,* upper-level parameters) and the vital rates that underline the matrix elements (*i.e.,* lower-level parameters), and note that their conversion is straightforward and described elsewhere (Franco & Silvertown 2004). The framework operates on three steps:

The first step of our framework involves acquiring the relative contribution of each demographic process to the stochastic growth rate, $\lambda_s$, the so-called stochastic elasticities, $E_{ij}^{S}$ (Tuljapurkar *et al.* 2003) (Figure 1A). The sum of all stochastic elasticities ($\Sigma E_{a_{ij}}^{S}$), can be separated into two components to assess how temporal variance and mean values of each demographic process contributes to $\lambda_s$. The first component represents the *sum of stochastic elasticity of $\lambda_s$ with respect to the variance* $\Sigma E_{a_{ij}}^{S^{\sigma}}$, and the second represents the *sum of stochastic elasticity of $\lambda_s$ with respect to the mean* $\Sigma E_{a_{ij}}^{S^{\mu}}$, where $\Sigma E_{a_{ij}}^{S} = \Sigma E_{a_{ij}}^{S^{\sigma}} + \Sigma E_{a_{ij}}^{S^{\mu}}$. Thus, the summation $\Sigma E_{a_{ij}}^{S^{\sigma}}$ quantifies the extent to which the stochastic population growth rate ($\lambda_s$) is influenced by changes in the variances of the demographic processes within the population matrix.

A higher sum of stochastic elasticity of $\lambda_s$ with respect to the variance (*i.e.,* higher absolute value; $|\Sigma E_{a_{ij}}^{S^{\sigma}}|$) indicates that small changes in the variance of demographic processes would have a substantial impact on $\lambda_s$. In other words, the variance of that demographic

process is not constrained by selection, supporting the DLH. On the other hand, a lower (absolute) stochastic elasticity of $\lambda_s$ with respect to the variance suggests that $\lambda_s$ is less sensitive to such perturbations, or, that variance of such demographic process is being constrained by natural selection, supporting the DBH (Tuljapurkar *et al.* 2003; Haridas & Tuljapurkar 2005) (Fig. 1A).

The first step of the framework thus features the interspecific level and places species or populations alongside a continuum. Species exhibiting unconstrained variance in the most important demographic process (*i.e.,* not buffered/potentially DLH suggesting, Fig. 1A, blue dots) are positioned on the left-hand side of the continuum. In contrast, species with constrained variance in the most important demographic process (*i.e.,* supporting the DBH, Fig. 1A, yellow dots) are positioned on the right-hand side of the continuum. However, the left-hand side of the continuum does not necessarily imply evidence of demographic lability. This is so because demographic lability is defined as an increase in the *mean value* of a demographic process in response to improved environmental conditions (Le Coeur *et al.* 2022). By examining $\Sigma E_{a_{ij}}^{S^\sigma}$, we can visualize an increase or decrease in *variance* of demographic processes, while the mean value of a demographic process does not change. The right-hand side (near 0 values for $\Sigma E_{a_{ij}}^{S^\sigma}$) supports the DBH, while the opposite end represents the lack of support for the DBH, and potentially support for the DLH. However, to undoubtedly provide support for the DLH, further investigation of demographic parameters is needed, as described below.

Step 1 of our framework examines the impacts that environmental variation has on the long-term population growth rate, $\lambda_s$ (Tuljapurkar *et al.* 2003). This means that the resulting variance continuum in this step of the framework is based on how $\lambda_s$ was affected by variation in the key demographic parameter across all contiguous time periods.

213 Steps 2 and 3 of the framework are conducted at the intraspecific level. Once species
214 or populations are positioned along the variance continuum regarding the most important
215 demographic process for $\lambda_s$, (step 1), one needs to zoom into each life cycle separately,
216 analysing the selection pressures acting on each one of the demographic processes composing
217 the life cycle. In doing so, one can inspect the selection pressures that have generated the
218 patterns found in step 1. Step 2 (Fig. 1B) requires obtaining the partial derivatives of the
219 deterministic population growth rate, $\lambda_t$, relative to all matrix elements of the MPM of interest
220 (*i.e.,* elasticities of $\lambda_t$ w.r.t each demographic process in the MPM). Step 2 therefore informs
221 on the strength of the natural selection on each of the demographic processes.
222 Finally, in step 3, one assesses the pattern of nonlinear selection by using the self-
223 second derivatives of $\lambda_t$ with respect to each demographic process (Fig. 1C). This final step
224 reveals the potential nonlinear selection pressures on all the demographic processes within a
225 life cycle, rather than only the most important one. This final step is key to understanding the
226 evolutionary processes (*i.e.,* types of nonlinear selection) that the demographic processes are
227 subjected to. Without understanding the evolutionary processes operating on the demographic
228 processes, the pattern observed in step 1 might be artefactual. Moreover, step 1 is founded on
229 the assumption that the importance of a demographic process, as indicated by its elasticity,
230 remains unchanged over time. However, stochastic environments can substantially alter
231 elasticity patterns throughout a life cycle (e.g., Lawler et al. 2009).
232 Steps 2 and 3 of the framework feature selection pressures that have been averaged
233 over the contiguous time periods. This means that the resulting patterns are based on how $\lambda_t$
234 (obtained from averaging all sequential MPMs across the duration of the study) would be
235 affected if a demographic process were perturbed. Therefore, steps 2 and 3 are based on a
236 different information than step 1, and can thus complete our understanding of the role of
237 selection pressures on shaping demographic patterns across multiple species.

238 Another important asset of step 3 above includes the notion that the relative
239 importance (elasticity) of demographic processes themselves changes with changing
240 environment (Stearns 1992). In other words, the extent to which $\lambda_t$ is sensitive to
241 perturbations in a specific demographic process is *dynamic* (Kroon, Hans *et al.* 2000). Thus, the
242 self-second derivatives generate information on how the sensitivity (or elasticity) of $\lambda_t$ –
243 based on which the entire variance continuum of species is produced in step 1 – might
244 change. If the sensitivity (or elasticity) of $\lambda_t$ can change, then it is important to know which
245 demographic processes are most prone to trigger such a change. In the example of a
246 hypothetical wolf species (Fig. 1), this means that if the reproduction of the third age-class
247 individuals (matrix element $a_{1,3}$) decreased, the sensitivity of $\lambda_t$ to $a_{1,3}$ would increase (square
248 with the largest black dot, Fig. 1C). Consequently, with increased environmental variability,
249 the key demographic process used to place this species onto the variance continuum in step 1
250 might change from remaining in the fourth age class (matrix element $a_{4,4}$, Fig. 1B) to
251 reproduction of the third age-class (matrix element $a_{1,3}$, Fig. 1C).
252 Combining the three steps of our framework allows for the clear, quantitative, holistic
253 identification of evidence to support (or reject) the DBH. Steps 2 and 3 offer key insights as
254 to *why* a given species or population is placed on either the buffered or the non-buffered
255 (potentially labile) end of the variance continuum. A clear and unequivocal evidence for
256 support towards the DBH consists of: (1) a species or population being positioned near the 0
257 end of the continuum (the right-hand side) in step 1; (2) this species' or populations' life
258 cycle having one or more demographic processes with highest elasticity values in step 2; and
259 (3) the same demographic process displaying the highest elasticity in step 2 with negative
260 self-second derivative values in step 3. In this sense, Figure 1B shows that, for the chosen
261 population of a hypothetical wolf species, the most important demographic process is
262 remaining in the fourth stage (MPM element $a_{4,4}$), as this demographic process results in

highest elasticity value (Fig. 1B yellow square). However, Fig. 1C reveals that $a_{4,4}$ is under little selection pressure for variance reduction. Thus, there is no evidence for DBH from the third step of the framework (*i.e.,* no concave selection forces), therefore, the lack of concave selection forces on the key demographic process within wolf's life cycle explains why this species is placed on the left-hand side of the variance continuum (Fig. 1A).

Species placed on the non-buffered end of the continuum is the first but not last step to evidence demographic lability. Indeed, locating a species on the non-buffered end of the variance continuum is a necessary but not sufficient condition for evidence in favour of the DLH. It is key highlighting here that demographic buffering and lability do not represent two extremes of the same continuum. The variance continuum allocates the species or populations from strongly buffered to non-buffered, but to test the DLH, a further step is needed.

Although not our primary goal here, we briefly introduce said step 4. To establish compelling evidence for or against the DLH, it is essential to fulfil several criteria. First, sufficient data across various environments (over time or space) are required to construct reaction norms that depict how a demographic process responds to environmental changes (Morris et al., 2008; Koons et al., 2009). Second, non-linear relationships between demographic processes and the environment must be established based on these reaction norms. Lastly, to identify demographic processes where an increase in the mean value has a stronger positive impact on population growth rate than the detrimental effect of increased variance. This latter condition is only achieved when the vital rate-environment reaction norm is convex (U-shaped; Morris et al. 2008; Koons et al. 2009). Importantly, we note that more likely than previously thought (*e.g.,* Pfister 1998), species do not exist as purely buffering or labile, but that within species, some vital rates may be buffered, other labile, and others insensitive to the environment (*e.g.*, Doak et al. 2005). Deciphering generality in this likely complex pattern should attract much research attention going forward, in our opinion.

## Demographic buffering in mammals: a case study using the unified framework

We demonstrate the performance of our framework using 44 MPMs from 34 mammal species. Mammals are of special interest here for two reasons: (1) mammalian life histories have been well studied (Gillespie 1977; Stearns 1983; Bielby *et al.* 2007; Jones 2011); and (2) some of their populations have already been assessed in terms of buffering, particularly for primates (Morris *et al.* 2008, 2011; Reed & Slade 2012; Rotella *et al.* 2012; Campos *et al.* 2017). Together, the well-studied life histories and previous information about the occurrence of buffering in mammals provide the necessary information to make accurate predictions and validate the performance of the proposed framework.

We used Matrix Population Models from 40 out of 139 studies with mammals available in the COMADRE database v.3.0.0 (Salguero-Gómez *et al.* 2016). These 40 populations encompass 34 species from eight taxonomic orders. We included these MPMs in our analyses because they provide values of demographic processes ($a_{ij}$) for three or more contiguous time periods, thus allowing us to obtain the stochastic elasticity of each $a_{ij}$. Although we are aware that not all possible temporal variation in demographic processes may have been expressed within this period, we assumed three or more transitions are enough to provide sufficient variation for population comparison. At least three contiguous time periods - a common selection criteria in comparative studies of stochastic demography (Compagnoni *et al.* 2023) - also allowed to test and showcase our framework. Fortunately, several long-lived species, characterized by low variation in their demographic processes, were studied for a long time (*e.g.,* some primates in our dataset have been studied for over 20 years – Morris *et al*. 2011). We removed the populations where either only survival or only reproduction rates were reported, because of the impossibility to calculate the stochastic growth rate. A detailed description of the analysed data and their original sources are available in supplementary material (Supplementary Material, Table S1).

*Homo sapiens* was included in our analyses because it is the only mammalian species in which second-order derivatives have been applied (Caswell 1996). Therefore, *Homo sapiens* provides an ideal basis for comparisons among species. The data for *Homo sapiens* were gathered from 26 modern populations located in various cities, allowing us to construct a spatiotemporal variance. It is important to note that in this case, we are not working with true temporal variance but rather a variance that encompasses both spatial and temporal aspects.

For steps 2 and 3 of our framework, we utilized a subset of 16 populations (including *Homo sapiens*) whose population projection matrices (MPMs) were organized by age. We specifically selected these populations because their life cycles can be summarized by two main demographic processes: survival and contribution to recruitment of new individuals. The contribution to recruitment can be interpreted as either the mean reproductive output for each age class or an approximation thereof, depending on how the matrices are structured (Ebert 1999). One advantage of using such matrices is that they encompass only two types of demographic processes, namely survival and recruitment, eliminating the need to account for multiple transitions between different life stages.

To perform the step 1 of our framework and obtain the $\Sigma E_{a_{ij}}^{S^{\sigma}}$ (and $\Sigma E_{a_{ij}}^{S^{\mu}}$), we followed Tuljapurkar *et al.* (2003). To perform step 2 of our framework, we calculated the deterministic elasticities of each demographic process extracted using the *popbio* package. All analyses were performed using R version 3.5.1 (R Core team, 2018). Finally, to perform the step 3 of our framework the self-second derivatives were adapted from *demogR* (Jones 2007) following Caswell 1996 and applied for the mean MPM.

*Results*

We ranked 40 populations from the 34 identified mammal species according to the cumulative impact of variation in demographic processes on $\lambda_s$ using the step 1 of our framework (Fig. 2). Additional information is provided in the supplementary material (Table S1). Most of the analysed orders were placed on the low-variance end of the variance continuum (Fig. 2). The smallest contributions of variation in demographic processes (*i.e.,* maximum value of $\Sigma E_{a_{ij}}^{S^\sigma}$, note that $\Sigma E_{a_{ij}}^{S^\sigma}$ ranges from 0 to -1), suggesting more buffered populations, were assigned to Primates: northern muriqui (*Brachyteles hyphoxantus*, $\Sigma E_{a_{ij}}^{S^\sigma}$ = -0.09 × $10^{-4}$ ± 0.12 × $10^{-4}$) (mean ± standard deviation) (Fig. 2 silhouette a), mountain gorilla (*Gorilla beringhei*, $\Sigma E_{a_{ij}}^{S^\sigma}$ = -0.24 × $10^{-4}$ ± 0.08 × $10^{-4}$) (Fig. 2 silhouette b), followed by the blue monkey (*Cercopithecus mitis*, $\Sigma E_{a_{ij}}^{S^\sigma}$ = -0.63 × $10^{-4}$ ± 0.06 × $10^{-4}$) (Fig. 2 silhouette c). The first non-primate species placed near the low-variance end of the continuum was the Columbian ground squirrel (*Urocitellus columbianus*, Rodentia, $\Sigma E_{a_{ij}}^{S^\sigma}$ = -0.003 ± 0.002) (Fig. 2 silhouette d). The species with the highest contribution of variation in demographic processes placed at the high-variance end of the continuum was the stoat (*Mustela erminea*, Carnivora, $\Sigma E_{a_{ij}}^{S^\sigma}$ = -0.35 ± 0.02) (Fig. 2 silhouette e). All the 14 primate populations supported the DBH, occupying the right-hand side of the variance continuum, with exception of the Patas monkey (*Erythrocebus patas*, Primates, $\Sigma E_{a_{ij}}^{S^\sigma}$ = -0.05 ± 0.03) (Fig. 2 silhouette f). The snowshoe hare (*Lepus americanus*, Lagomorpha, $\Sigma E_{a_{ij}}^{S^\sigma}$ = -0.29 ± 0.16) (Fig. 2 silhouette g) and the Bush rat (*Rattus fuscipes*, Rodentia, $\Sigma E_{a_{ij}}^{S^\sigma}$ = -0.25 ± 0.03) (Fig. 2 silhouette h) appear on the high-variance end of the continuum.

As predicted for the steps 2 and 3, we could not observe a clear pattern in support of the DBH. This finding means that the demographic processes with the highest elasticity values failed to display strongly negative self-second derivatives (Fig. 3). Particularly for

majority of primates - with the lack or minor temporal variation in demographic processes - demographic processes with high elasticities had positive values for the self-second derivatives (indicated by yellow squares with white dots in Fig. 3). Examples of primate species exhibiting high elasticities and positive values for the self-second derivatives and include northern muriqui (*Brachyteles hypoxanthus*), mountain gorilla (*Gorilla beringei*), white-faced capuchin monkey (*Cebus capucinus*), rhesus monkey (*Macaca mulatta*), blue monkey (*Cercopithecus mitis*), Verreaux's sifaka (*Propithecus verreauxi*) and olive baboon (*Papio cynocephalus*) (Fig. 3). This implies that the key demographic processes influencing $\lambda_t$ are not subject to selective pressure for reducing their temporal variability. However, even though the primates were positioned closer to the low-variance end of the continuum in step 1, the evidence from steps 2 and 3 does not support DBH.

The killer whale showed similar controversy between step 1 and steps 2-3 results as most primates. In step 1, the killer whale was positioned at the buffered end of the variance continuum (*Orcinus orca*, Cetacea, $\Sigma E_{a_{ij}}^{S^\sigma} = -0.70 \times 10^{-4} \pm 1.04 \times 10^{-5}$) (Fig. 2 silhouette not shown). However, steps 2 and 3 show that the three demographic processes in killer whale life cycle with highest elasticity values (matrix elements $a_{2,2}$, $a_{3,3}$ and $a_{4,4}$) are not under selection pressures for reducing their temporal variance, but the opposite (depicted by yellow and green squares with white dots, Fig. 3).

The only primate species exhibiting DBH evidence in steps 2 and 3 was human. In human, demographic parameters representing survival from first to second age class (matrix element $a_{2,1}$) displayed high elasticities and negative self-second derivatives (depicted as yellow squares with black dots in Fig. 3). Evidence supporting the DBH was also found in the Columbian ground squirrel (*Urocitellus columbianus*), where, similar to humans, survival from the first to the second age class (matrix element $a_{2,1}$) showed indications of selection acting to reduce its variance. Accordingly, the Columbian ground squirrel was positioned

385 close to the buffered end of the variance continuum in step 1. Hence, the Columbian ground
386 squirrel was the sole species with consistent DBH support across all three steps of the
387 framework.

388 The Soay sheep (*Ovis aries*) was the species furthest from the buffered end of the
389 variance continuum that enabled to perform steps 2 and 3. For the Soay sheep, remaining in
390 the third age class (matrix element $a_{3,3}$) has the major influence on $\lambda_t$ and is under selection
391 pressure to have its variance increased. The latter characteristics reveal conditions for the
392 DLH support even though the species is placed closer to the buffered end of the variance
393 continuum.

394 Steps 2 and 3 illustrate the importance of examining DBH evidence on the
395 intraspecific level. These two steps of the framework identify the simultaneous acting of
396 concave and convex selection on different demographic processes but within a single life
397 cycle. In polar bear (*Ursus maritimus*), the key demographic process (matrix element $a_{4,4}$) is
398 under convex selection, as depicted by a yellow square with a white dot in Fig. 3. However,
399 the demographic process with the second highest elasticity value (matrix element $a_{5,4}$) is
400 under strong concave selection (depicted by a light green square with a black dot in Fig. 3).

401 By adding step 3 to the framework, another important information was added. The
402 high absolute values of self-second derivatives (large dots, either black or white, Fig. 3)
403 indicate where the sensitivity of $\lambda_t$ to demographic parameters is itself prone to environmental
404 changes. For instance, if the value of $a_{5,4}$ for polar bear increased, the sensitivity of $\lambda_t$ to $a_{5,4}$
405 would decrease because the self-second derivative of $a_{5,4}$ is highly negative (depicted by the
406 largest black dot in polar bear MPM). Vice versa holds for the $a_{4,4}$ demographic process,
407 where an increase in the value of $a_{4,4}$ would increase $\lambda_t$'s sensitivity to $a_{4,4}$, because the self-
408 second derivative of $a_{5,4}$ is highly positive (depicted by the largest white dot in polar bear

409 MPM). Thus, sensitivities (or equally elasticities) of demographic processes with high
410 absolute values for self-second derivatives can easily change - potentially changing the key
411 demographic process used for allocating species into the variance continuum in step 1 of the
412 framework.

413 **Discussion**

414 In the Anthropocene, identifying and quantifying mechanisms of species responses to
415 stochastic environments holds crucial importance. This importance is particularly tangible in
416 the context of the unprecedented environmental changes and uncertainties that impact the
417 dynamics and persistence of natural populations (Boyce *et al.* 2006). Correlational
418 demographic analysis, whereby the importance of demographic processes and their temporal
419 variability is examined (e.g., Pfister 1998), has attempted to identify how species may buffer
420 against the negative effects of environmental stochasticity. However, these widely used
421 approaches have important limitations (see Introduction and Hilde et al. 2020). Our novel
422 framework overcomes said limitations by providing a rigorous approach to test the
423 demographic buffering hypothesis (DBH; Pfister 1998; Hilde et al. 2020).

424 Evidencing demographic buffering is not straightforward. Indeed, through the
425 analysis of stochastic population growth rate ($\lambda_s$) in our application of the framework to 44
426 populations of 34 species, we identify the highest density of natural populations near the
427 buffered end of the variance continuum (step 1), indicating possible support for the DBH.
428 However, we show that the same species then fail to exhibit signs of concave (∩-shaped)
429 selection on the key demographic parameters when further analyses are performed averaging
430 the variation across the duration of each study (steps 2 and 3). This finding confirms that
431 placing the species near the buffered end of the variance continuum is *necessary* but not
432 *sufficient* to test the DBH. Indeed, buffering occurs when concave selection forces act on the
433 key demographic parameter (Caswell 1996, 2001; Shyu & Caswell 2014).

Combining the three steps into a unified framework is of outmost importance. In steps 2 and 3 of the framework, we find relatively limited overall support for the DBH in the examination of our 16 (out of 34 in step 1) studied animal species. Step 3 of our framework reveals that the role of natural selection shaping temporal variation in demographic processes is more complex than expected by the DBH alone. Indeed, demographic processes within our study populations are often under a mix of convex and concave selection. This mix of selection patterns was already suggested by Doak *et al.* (2005). Here, only two out of 16 mammal species revealed concave selection acting on the key demographic processes (Columbian ground squirrel [*Urocitellus columbianus*], and humans, [*Homo sapiens sapiens*]). These two species were also placed near the buffered end of the variance continuum, therefore meeting all the necessary conditions to diagnose clear support in favour of DBH. However, finding 12.5% (two out of 16) species that meet the criteria for demographic buffering is not in concordance with previous studies. Support for the DBH has been reported across 22 ungulate species (Gaillard & Yoccoz 2003). In the one ungulate we examined, the moose (*Alces alces*), we find only partial support for DBH in adult survival, since this species is placed near the buffered end of the variance continuum in step 1 but does not show concave selection pressures on adult survival in step 2/3, as predicted by the DBH.

Our overall findings reveal varying levels of support for the notion that adult survival in long-lived species tends to be buffered. Indeed, Gaillard *et al.* (1998) found that adult female survival varied considerably less than juvenile survival in large herbivores. This finding was also supported by further studies in ungulates (Gaillard & Yoccoz 2003), turtles (Heppell 1998), vertebrates and plants (Pfister 1998), and more recently across nine (out of 73) species of plants (McDonald *et al.* 2017).

When placing our study species along a variance continuum (step 1), primates tend to be located on the buffered end. However, most primates displayed convex –instead of the

459 expected concave– selection on adult survival. Similar results, where the key demographic
460 process failed to display constrained temporal variability, have been reported for long-lived
461 seabirds (Doherty *et al.* 2004). One explanation for the unexpected convex selection on adult
462 survival involves trade-offs, as suggested by Doak et al. (2005). When two demographic
463 parameters are negatively correlated, the variance of population growth rate ($\lambda$) can be
464 increased or decreased (Evans & Holsinger 2012; Compagnoni *et al.* 2016). The well-established
465 trade-off between survival and fecundity (e.g., Stearns 1992; Roff & Fairbairn 2007) might
466 explain the observed concave selection signatures on late fecundity and convex selection on
467 adult survival. Because variation in primate recruitment is already constrained by
468 physiological limitations (Campos *et al.* 2017), when adult survival and recruitment are
469 engaged in a trade-off, this trade-off might lead to our unexpected result. Here, future studies
470 may benefit from deeper insights via cross-second derivatives (Caswell 1996, 2001) to
471 investigate correlations among demographic processes.

472 Examining the drivers of demographic buffering has become an important piece of the
473 ecological and evolutionary puzzle of demography. As such, testing the DBH can help us
474 better predict population responses to environmental variability, climate change, and direct
475 anthropogenic disturbances (Pfister 1998; Boyce *et al.* 2006; McDonald *et al.* 2017; Vázquez *et al.*
476 2017). By setting the DBH into a broader and integrated framework, we hope to enhance
477 comprehension and prediction of the implications of heightened environmental stochasticity
478 on the evolution of life history traits. This understanding is crucial in mitigating the risk of
479 extinction for the most vulnerable species.

480

481 **Acknowledgements**

482 This study was financed in part by the *Coordenação de Aperfeiçoamento de Pessoal de Nível*
483 *Superior* - Brasil (CAPES) - Finance Code 001. GSS was supported by CAPES and CNPq

(301343/2023-3). RS-G was supported by a NERC Independent Research Fellowship (NE/M018458/1). MK was supported by the European Commission through the Marie Skłodowska-Curie fellowship (MSCA MaxPersist #101032484) hosted by RSG.

## Data availability

The demographic data used in this paper are open-access and available in the COMPADRE Plant Matrix Database (v. 5.0.1; https://compadre-db.org/Data/ Compadre). A list of the studies and species used here is available in Supplementary Material (Table S1). If the manuscript is accepted, the data and code supporting the results will be archived on Zenodo. The data and code specific DOI will then be included in our "Data availability" statement.

## References

Barraquand, F. & Yoccoz, N.G. (2013). When can environmental variability benefit population growth? Counterintuitive effects of nonlinearities in vital rates. *Theor Popul Biol*, 89, 1–11.

Bielby, J., Mace, G.M., Bininda-Emonds, O.R.P., Cardillo, M., Gittleman, J.L., Jones, K.E., *et al.* (2007). The Fast-Slow Continuum in Mammalian Life History: An Empirical Reevaluation. *Am Nat*, 169, 748–757.

Bonsall, M.B. & Klug, H. (2011). The evolution of parental care in stochastic environments. *J Evol Biol*, 24, 645–655.

Boyce, M.S., Haridas, C. V., Lee, C.T., Boggs, C.L., Bruna, E.M., Coulson, T., *et al.* (2006). Demography in an increasingly variable world. *Trends Ecol Evol*, 21, 141–148.

Brodie, E.I., Moore, A. & Janzen, F. (1995). Visualizing and quantifying natural selection. *Trends Ecol Evol*, 10, 313–318.

Campos, F.A., Morris, W.F., Alberts, S.C., Altmann, J., Brockman, D.K., Cords, M., *et al.* (2017). Does climate variability influence the demography of wild primates? Evidence from long-term life-history data in seven species. *Glob Chang Biol*, 23, 4907–4921.

Carslake, D., Townley, S. & Hodgson, D.J. (2008). Nonlinearity in eigenvalue-perturbation curves of simulated population projection matrices. *Theor Popul Biol*, 73, 498–505.

Caswell, H. (1996). Second Derivatives of Population Growth Rate: Calculation and Applications. *Ecology*, 77, 870–879.

Caswell, H. (2001). *Matrix Population Models: Construction, Analysis, and Interpretation*. Sinauer Associates Inc. Publishers, Sunderland, Massachusetts, USA.

Charlesworth, B. (1994). *Evolution in age-structured populations*. second edi. Cambridge University Press.

Le Coeur, C., Yoccoz, N.G., Salguero-Gómez, R. & Vindenes, Y. (2022). Life history adaptations to fluctuating environments: Combined effects of demographic buffering and lability. *Ecol Lett*, 1–13.

Compagnoni, A., Bibian, A.J., Ochocki, B.M., Rogers, H.S., Schultz, E.L., Sneck, M.E., *et al.* (2016). The effect of demographic correlations on the stochastic population dynamics of perennial plants. *Ecol Monogr*, 86, 480–494.

Compagnoni, A., Evers, S. & Knight, T. (2023). Spatial replication can best advance our understanding of population responses to climate. *bioRxiv*, https://doi.org/10.1101/2022.06.24.497542.

Doak, D.F., Morris, W.F., Pfister, C., Kendall, B.E. & Bruna, E.M. (2005). Correctly Estimating How Environmental Stochasticity Influences Fitness and Population Growth. *Am Nat*, 166, E14–E21.

Doak, D.F., Waddle, E., Langendorf, R.E., Louthan, A.M., Isabelle Chardon, N., Dibner, R.R., *et al.* (2021). A critical comparison of integral projection and matrix projection models for demographic analysis. *Ecol Monogr*, 91, e01447.

Doherty, P.F., Schreiber, E.A., Nichols, J.D., Hines, J.E., Link, W.A., Schenk, G.A., *et al.* (2004). Testing life history predictions in a long-lived seabird: A population matrix approach with improved parameter estimation. *Oikos*, 105, 606–618.

Easterling, M.R., Ellner, S.P. & Dixon, P.M. (2000). Size-Specific Sensitivity: Applying a New Structured Population Model. *Ecology*, 81, 694–708.

Ellner, S.P., Childs, D.Z. & Rees, M. (2016). Data-driven Modelling of Structured Populations.

Evans, M.E.K. & Holsinger, K.E. (2012). Estimating covariation between vital rates : A simulation study of connected vs . separate generalized linear mixed models (GLMMs). *Theor Popul Biol*, 82, 299–306.

Ferreira, M., Kajin, M., Vieira, M., Zangrandi, P., Cerqueira, R. & Gentile, R. (2013). Life history of a neotropical marsupial: Evaluating potential contributions of survival and reproduction to population growth rate. *Mamm Biol*, 78, 406–411.

Franco, M. & Silvertown, J. (2004). A comparative demography of plants based upon elasticities of vital rates. *Ecology*, 85, 531–538.

Gaillard, J.-M. & Yoccoz, N. (2003). Temporal Variation in Survival of Mammals: a Case of Environmental Canalization? *Ecology*, 84, 3294–3306.

Gillespie, J.H. (1977). Natural Selection for Variances in Offspring Numbers: A New Evolutionary Principle. *Am Nat*, 111, 1010–1014.

Griffith, A.B. (2017). Perturbation approaches for integral projection models. *Oikos*, 126, 1675–1686.

Haridas, C.V. & Tuljapurkar, S. (2005). Elasticities in Variable Environments: Properties and Implications. *Am Nat*, 166, 481–495.

Healy, K., Ezard, T.H.G., Jones, O.R., Salguero-Gómez, R. & Buckley, Y.M. (2019). Animal life history is shaped by the pace of life and the distribution of age-specific mortality and reproduction. *Nat Ecol Evol*, 3, 1217–1224.

556 Heppell, S.S. (1998). Application of Life-History Theory and Population Model Analysis to Turtle
557 Conservation. *Copeia*, 1998, 367.

558 Hilde, C.H., Gamelon, M., Sæther, B.-E., Gaillard, J.-M., Yoccoz, N.G. & Pélabon, C. (2020). The
559 Demographic Buffering Hypothesis: Evidence and Challenges. *Trends Ecol Evol*, 35, 523–538.

560 Jäkäläniemi, A., Ramula, S. & Tuomi, J. (2013). Variability of important vital rates challenges the
561 demographic buffering hypothesis. *Evol Ecol*, 27, 533–545.

562 Jones, J.H. (2007). Journal of Statistical Software, 22.

563 Jones, J.H. (2011). Primates and the evolution of long, slow life histories. *Current Biology*, 21, R708–
564 R717.

565 Jongejans, E., De Kroon, H., Tuljapurkar, S. & Shea, K. (2010). Plant populations track rather than
566 buffer climate fluctuations. *Ecol Lett*, 13, 736–743.

567 Koons, D.N., Pavard, S., Baudisch, A. & Jessica E. Metcalf, C. (2009). Is life-history buffering or
568 lability adaptive in stochastic environments? *Oikos*, 118, 972–980.

569 Kroon, Hans, D., van Groenendael, J. & Ehrlen, J. (2000). Elasticities: A review of methods and
570 model limitations.

571 Lawler, R.R., Caswell, H., Richard, A.F., Ratsirarson, J., Dewar, R.E. & Schwartz, M. (2009).
572 Demography of Verreaux's sifaka in a stochastic rainfall environment. *Oecologia*, 161, 491–
573 504.

574 McDonald, J.L., Franco, M., Townley, S., Ezard, T.H.G., Jelbert, K. & Hodgson, D.J. (2017).
575 Divergent demographic strategies of plants in variable environments. *Nat Ecol Evol*, 1, 0029.

576 Morris, W.F., Altmann, J., Brockman, D.K., Cords, M., Fedigan, L.M., Pusey, A.E., *et al.* (2011).
577 Low Demographic Variability in Wild Primate Populations: Fitness Impacts of Variation,
578 Covariation, and Serial Correlation in Vital Rates. *Am Nat*, 177, E14–E28.

579 Morris, W.F. & Doak, D.F. (2004). Buffering of Life Histories against Environmental Stochasticity:
580 Accounting for a Spurious Correlation between the Variabilities of Vital Rates and Their
581 Contributions to Fitness. *Am Nat*, 163, 579–590.

582 Morris, W.F., Pfister, C.A., Tuljapurkar, S., Haridas, C. V., Boggs, C.L., Boyce, M.S., *et al.* (2008).
583 Longevity can buffer plant and animal populations against changing climatic variability.
584 *Ecology*, 89, 19–25.

585 Pélabon, C., Hilde, C.H., Einum, S. & Gamelon, M. (2020). On the use of the coefficient of variation
586 to quantify and compare trait variation. *Evol Lett*, 4, 180–188.

587 Pfister, C. (1998). Patterns of variance in stage-structured populations: Evolutionary predictions and
588 ecological implications. *Proceedings of the National Academy of Sciences*, 95, 213–218.

589 Reed, A.W. & Slade, N.A. (2012). Buffering and plasticity in vital rates of oldfield rodents. *Journal*
590 *of Animal Ecology*, 81, 953–959.

591 Rodríguez-Caro, R.C., Capdevila, P., Graciá, E., Barbosa, J.M., Giménez, A. & Salguero-Gómez, R.
592 (2020). The demographic buffering strategy has a threshold of effectiveness to increases in
593 environmental stochasticity. *bioRxiv*, 1–41.

594 Roff, D.A. & Fairbairn, D.J. (2007). The evolution of trade-offs: Where are we? *J Evol Biol*, 20, 433–
595 447.

Rotella, J.J., Link, W.A., Chambert, T., Stauffer, G.E. & Garrott, R.A. (2012). Evaluating the demographic buffering hypothesis with vital rates estimated for Weddell seals from 30 years of mark – recapture data, 162–173.

Salguero-Gómez, R., Jones, O.R., Archer, C.R., Bein, C., de Buhr, H., Farack, C., *et al.* (2016). COMADRE: A global data base of animal demography. *Journal of Animal Ecology*, 85, 371–384.

Shyu, E. & Caswell, H. (2014). Calculating second derivatives of population growth rates for ecology and evolution. *Methods Ecol Evol*, 5, 473–482.

Stearns, S. (1992). *The Evolution of Life Histories*. Oxford University Press, New York, USA.

Stearns, S.C. (1983). The Influence of Size and Phylogeny on Patterns of Covariation among Life-History Traits in the Mammals. *Oikos*, 41, 173.

Sutherland, W.J., Freckleton, R.P., Godfray, H.C.J., Beissinger, S.R., Benton, T., Cameron, D.D., *et al.* (2013). Identification of 100 fundamental ecological questions. *Journal of Ecology*, 101, 58–67.

Tuljapurkar, S., Gaillard, J.-M. & Coulson, T. (2009). From stochastic environments to life histories and back. *Philosophical Transactions of the Royal Society B: Biological Sciences*, 364, 1499–1509.

Tuljapurkar, S., Horvitz, C.C. & Pascarella, J.B. (2003). The Many Growth Rates and Elasticities of Populations in Random Environments. *Am Nat*, 162, 489–502.

Vázquez, D.P., Gianoli, E., Morris, W.F. & Bozinovic, F. (2017). Ecological and evolutionary impacts of changing climatic variability. *Biological Reviews*, 92, 22–42.

Wang, J., Yang, X., Silva Santos, G., Ning, H., Li, T., Zhao, W., *et al.* (2023). Flexible demographic strategies promote the population persistence of a pioneer conifer tree (Pinus massoniana) in ecological restoration. *For Ecol Manage*, 529, 120727.

622 **Figure 1**

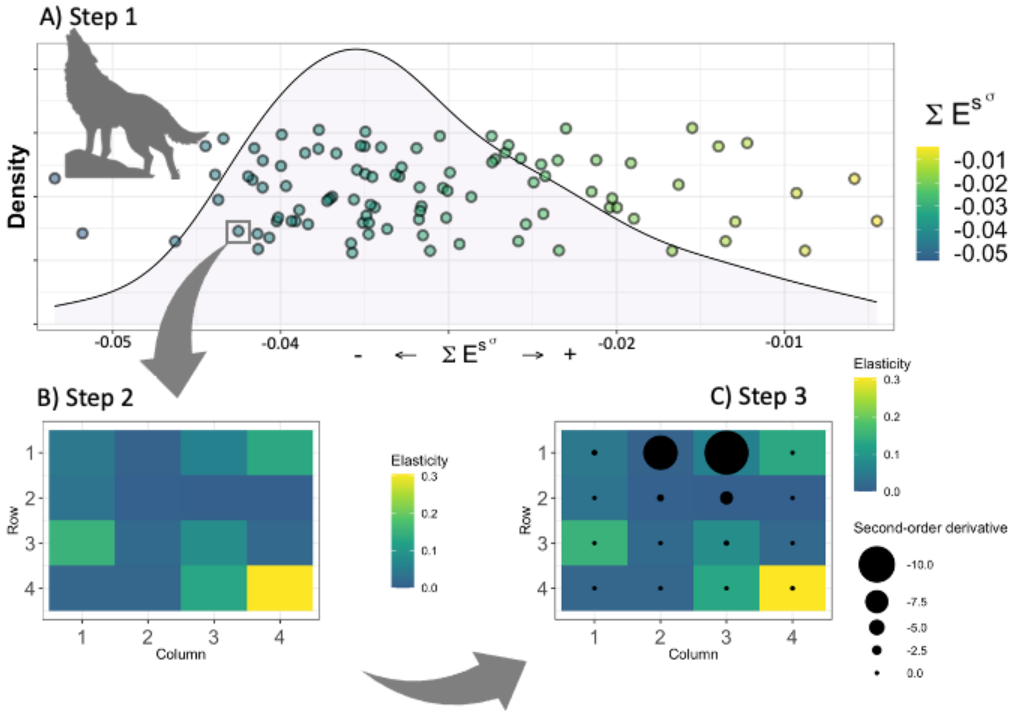


623

624 **Figure 2**

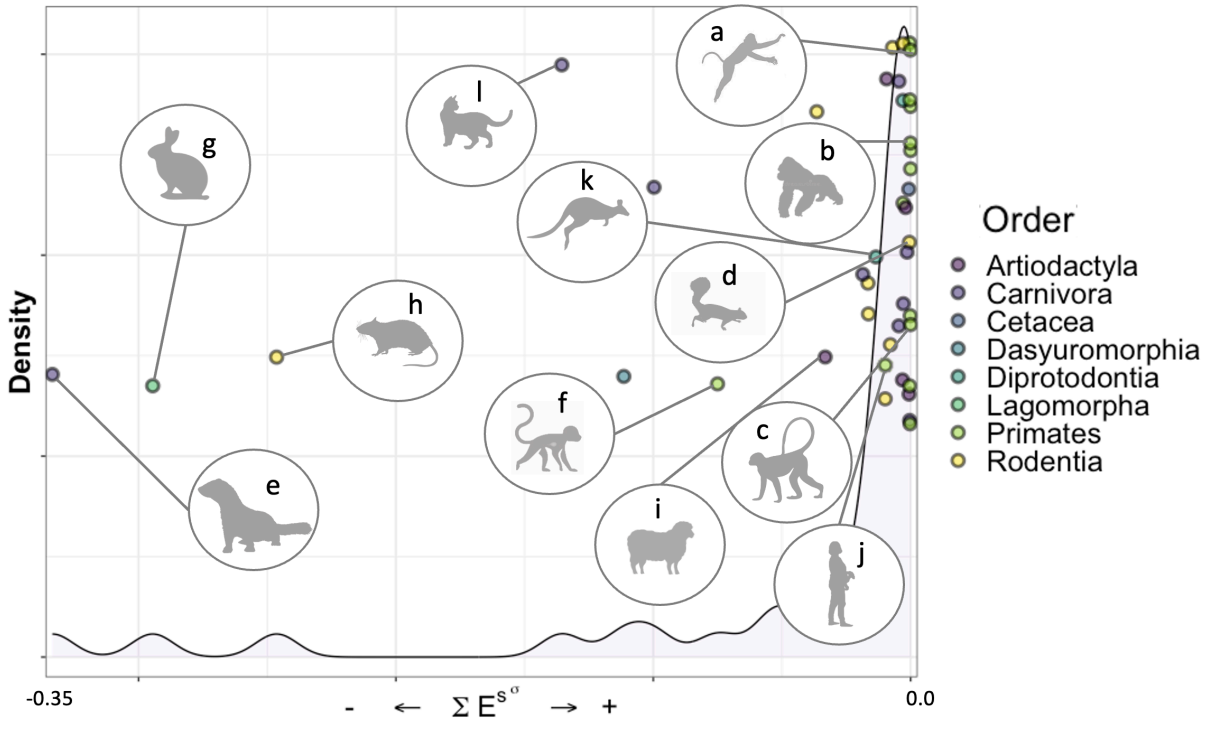


625

626

627 **Figure 3**

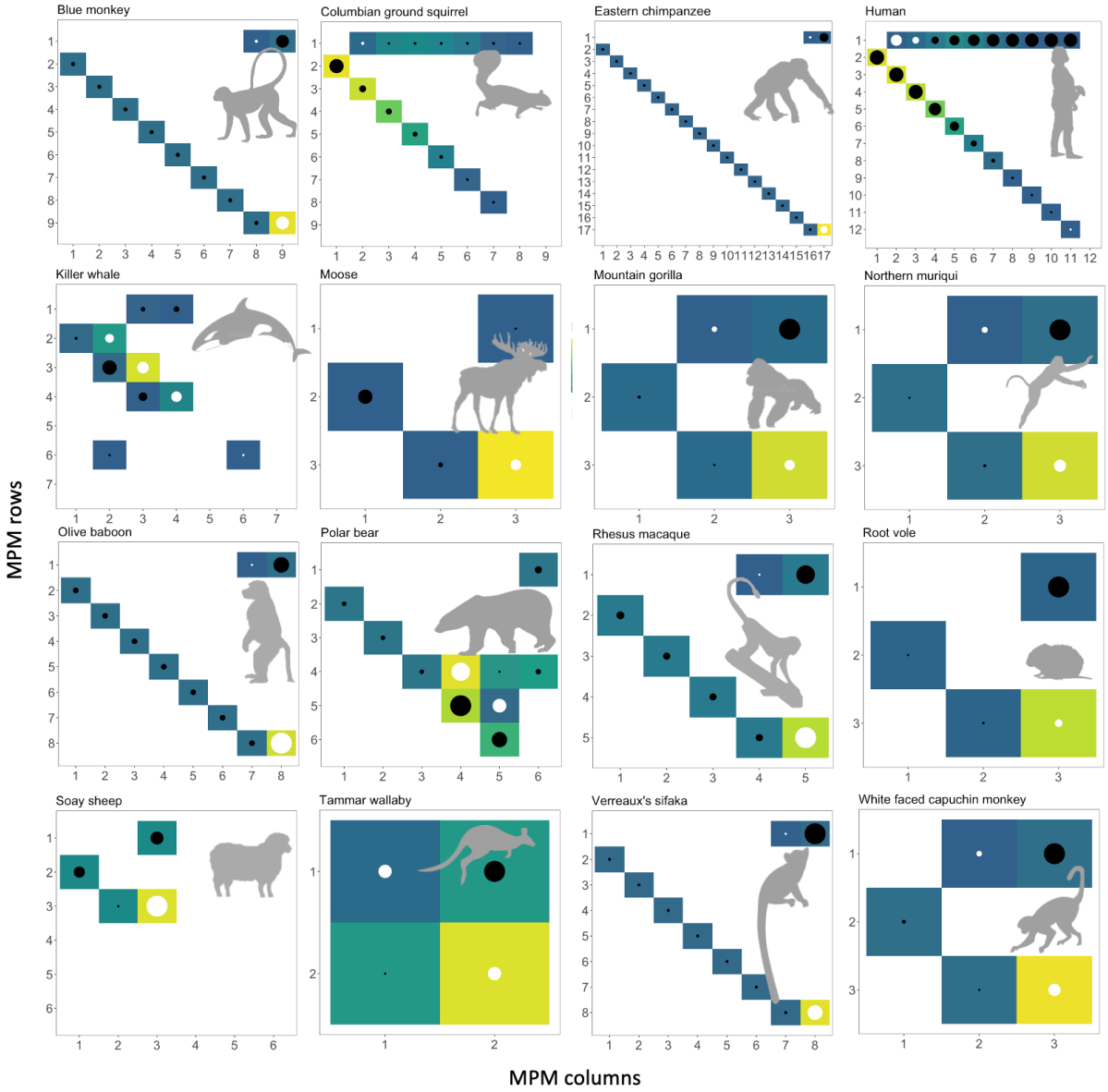


628

629

630

631 **Figure legends**

632

633 **Figure 1**. A three-step framework proposed to: Step 1 - allocate species and/or populations
634 on a variance continuum (plot A, dots representing 50 hypothetical species). The variance
635 continuum operates at the interspecific level (see text) and is represented by partitioning the
636 sum of all the stochastic elasticities ($\Sigma E^{S}_{a_{ij}}$) into two compounds: i) sums of stochastic
637 elasticities with respect to the variance ($\Sigma E^{S^{\sigma}}_{a_{ij}}$), and ii) sums of stochastic elasticities with
638 respect to the mean ($\Sigma E^{S^{\mu}}_{a_{ij}}$). The first step of our framework shows the variance compound of
639 the sums of stochastic elasticities forming a continuum where the right-hand side of the plot
640 represents species (or populations) where a perturbation of variance of the most important
641 demographic process results in weak or no impact on $\lambda_s$ (yellow dots). The yellow-dotted
642 species (or populations) can be classified as having *buffered life-cycles (supporting the DBH)*
643 – based on the most important demographic process for the $\lambda_s$. The left-hand side of the graph
644 represents species (or populations) where a perturbation of the variance of the most important
645 demographic process results in strong impact on $\lambda_s$ (blue dots). Thus, the blue-dotted species
646 (or populations) can be classified as having *unbuffered life cycles (potentially supporting*
647 *DLH,* see text) – based on the most important demographic process for the $\lambda_s$. The jitter
648 applied on the y-axis has no biological meaning. Step 2 - Access the linear selection
649 pressures for individual species or populations at intraspecific level (see text) (plot B). Step 2
650 displays the elasticities of the deterministic population growth rate ($\lambda_t$) for a hypothetical
651 population of wolf and reveals the linear selection gradients. Step 3 - Access the nonlinear
652 selection pressures at the intraspecific level (see text) (plot C). In the third step self-second
653 derivatives for the corresponding demographic processes from step 2 are displayed.

654

**Figure 2**. Results for step 1 of our framework showing the sum of stochastic elasticities with respect to the variance $\Sigma E_{a_{ij}}^{S^{\sigma}}$ increase caused by a perturbation in the most relevant demographic process. The 40 populations from 34 species of mammals from the COMADRE database are ranked into the variance continuum from strongly buffered (right-hand side, supporting the DBH) to more variable, less buffered (left-hand side, potentially supporting the DLH, see text). Colors represent different taxonomic orders with Primates occupying the right-hand side. Silhouettes: a) *Brachyteles hyphoxantus*, b) *Gorilla beringhei*, c) *Cercopithecus mitis*, d) *Urocitellus columbianus,* e) *Mustela erminea*, f) *Erythrocebus patas*, g) *Lepus americanus*, h) *Rattus fuscipes*, i) *Ovis aries*, j) *Homo sapiens*, k) *Macropus eugenii*, and l) *Felis catus*. The jitter applied on the y-axis has no biological meaning.

**Figure 3:** Results from steps 2 and 3 of the proposed framework (see Fig. 2B, C). The 16 plots represent populations where the MPMs built by ages were available in the COMADRE database (see text). The color scale represents elasticity values for each of the demographic processes in the MPM, where yellow represents high and blue low elasticity values. No color means elasticity=0. Because the aim of step 2 is to identify the most important demographic process within each species' life cycle (the intraspecific level, see text) - not to compare the elasticity values among species - each plot has its own scale (see end of legend). The black dots represent negative self-second derivatives of $\lambda_t$ - thus concave selection - and the white dots represent positive self-second derivatives of $\lambda_t$ - thus convex selection. The dot sizes are scaled by the absolute value of self-second derivatives, where the smaller the dot, the closer a self-second derivative is to 0, indicting weak or no selection. Large dots indicate strong selection forces. Scales ($E_{min\text{-}max}$=elasticity minimum and maximum value, $SSD_{min\text{-}max}$=self-second derivative minimum and maximum value): Blue monkey $E_{min\text{-}max}$=0.00-0.52, $SSD_{min\text{-}max}$=-1.25-1.27; Columbian ground squirrel: $E_{min\text{-}max}$=0.00-0.23, $SSD_{min\text{-}max}$=-1.48-0.01;

680 Eastern chimpanzee: $E_{min-max}$=0.00-0.60, $SSD_{min-max}$=-4.39-2.59; Human: $E_{min-max}$=0.00-0.18,
681 $SSD_{min-max}$=-0.15-0.08; Killer whale: $E_{min-max}$=0.00-0.55, $SSD_{min-max}$=-5.72-3.43; Moose:
682 $E_{min-max}$=0.00-0.55, $SSD_{min-max}$=-0.66-0.36; Mountain gorilla: $E_{min-max}$=0.00-0.81, $SSD_{min-max}$=-1.46-0.28; Northern muriqui: $E_{min-max}$=0.00-0.72, $SSD_{min-max}$=-1.17-0.35; Olive baboon:
684 $E_{min-max}$=0.00-0.54, $SSD_{min-max}$=-0.57-1.13; Polar bear: $E_{min-max}$=0.00-0.26, $SSD_{min-max}$=-
685 0.73-0.54; Rhesus macaque: $E_{min-max}$=0.00-0.51, $SSD_{min-max}$=-0.54-0.71; Root vole: $E_{min-max}$=0.00-0.86, $SSD_{min-max}$=-2.54-0.22; Soay sheep: $E_{min-max}$=0.00-0.56, $SSD_{min-max}$=-0.22-
687 0.40; Tammar wallaby: $E_{min-max}$=0.00-0.55, $SSD_{min-max}$=-0.64-0.34; White faced capuchin
688 monkey: $E_{min-max}$=0.00-0.66, $SSD_{min-max}$=-2.66-1.21.
689

690 **Supplementary material – Data available in COMADRE Version 2.0.1 and results from Step 1 of the framework**

691 **Table S1.** The metadata used in step 1 of our framework and the respective results presented in the main text. The first four columns represent
692 the information from where Matrix Populations Models (MPMs) were extract precisely as presented in COMADRE 2.0.1. Column titles differ
693 from the database as "SpeciesAuthorComadre" is equivalent to "SpeciesAuthor" and "SpeciesName" is equivalent to "SpeciesAccepted" in
694 COMADRE 2.0.1. The remaining columns present the results of step 1, where we present the raw values of $\Sigma E_{a_{ij}}^{S^{\mu}}$ and $\Sigma E_{a_{ij}}^{S^{\sigma}}$, their respective
695 standard deviation, the stochastic population growth rate $\lambda_s$, and the number of available matrices (# matrices). For ByAge, "TRUE" was
696 assigned for MPMs built by age or "FALSE" if otherwise.

| **SpeciesAuthorComadre** | **SpeciesName** | **CommonName** | **Order** | $\Sigma E_{a_{ij}}^{S^{\mu}}$ | $\Sigma E_{a_{ij}}^{S^{\mu}}$ **(sd)** | $\Sigma E_{a_{ij}}^{S^{\sigma}}$ | $\Sigma E_{a_{ij}}^{S^{\sigma}}$ **(sd)** | **# matrices** | $\lambda$ |
|---|---|---|---|---|---|---|---|---|---|
| Homo_sapiens_subsp._sapiens | *Homo sapiens sapiens* | Human | Primates | 1.003 | 0.003 | 1.003 | 0.004 | 13 | 1.064 |
| Alces_alces | *Alces alces* | Moose | Artiodactyla | 1.001 | 0.001 | 1.001 | 0.001 | 13 | 1.205 |
| Antechinus_agilis | *Antechinus agilis* | Agile antechinus | Dasyuromorphia | 1.111 | 0.111 | 1.111 | 0.011 | 2 | 0.931 |
| Brachyteles_hypoxanthus | *Brachyteles hypoxanthus* | Northern muriqui | Primates | 1.000 | 0.000 | 1.000 | 0.000 | 12 | 1.051 |
| Callospermophilus_lateralis | *Callospermophilus lateralis* | Golden-mantled ground squirrel | Rodentia | 1.054 | 0.054 | 1.054 | 0.055 | 9 | 2.052 |
| Cebus_capucinus | *Cebus capucinus* | White faced capuchin monkey | Primates | 1.000 | 0.000 | 1.000 | 0.000 | 11 | 1.021 |
| Cercopithecus_mitis | *Cercopithecus mitis* | Blue monkey | Primates | 1.000 | 0.000 | 1.000 | 0.000 | 14 | 1.036 |
| Eumetopias_jubatus | *Eumetopias jubatus* | Northern sea lion; Steller sea lion | Carnivora | 1.005 | 0.005 | 1.005 | 0.002 | 2 | 0.904 |
| Felis_catus | *Felis catus* | Feral cat | Carnivora | 1.136 | 0.136 | 1.136 | 0.012 | 1 | 1.948 |
| Gorilla_beringei | *Gorilla beringei* | Mountain gorilla | Primates | 1.000 | 0.000 | 1.000 | 0.000 | 21 | 1.027 |
| Hippocamelus_bisulcus | *Hippocamelus bisulcus* | Huemul deer | Artiodactyla | 1.002 | 0.002 | 1.002 | 0.001 | 1 | 0.996 |
| Lepus_americanus | *Lepus americanus* | Snowshoe hare | Lagomorpha | 1.294 | 0.294 | 1.294 | 0.165 | 2 | 0.812 |
| Lycaon_pictus | *Lycaon pictus* | African wild dog | Carnivora | 1.100 | 0.100 | 1.100 | 0.008 | 1 | 1.500 |
| Macaca_mulatta_3 | *Macaca mulatta* | Rhesus macaque | Primates | 1.000 | 0.000 | 1.000 | 0.001 | 12 | 1.127 |
| Macropus_eugenii | *Macropus eugenii* | Tammar wallaby | Diprotodontia | 1.013 | 0.013 | 1.013 | 0.012 | 7 | 0.981 |

| | | | | | | | | | |
|---|---|---|---|---|---|---|---|---|---|
| Marmota_flaviventris_2 | *Marmota flaviventris* | Yellow-bellied marmot | Rodentia | 1.007 | 0.007 | 1.007 | 0.006 | 4 | 0.890 |
| Marmota_flaviventris_3 | *Marmota flaviventris* | Yellow-bellied marmot | Rodentia | 1.008 | 0.008 | 1.008 | 0.005 | 4 | 0.921 |
| Microtus_oeconomus | *Microtus oeconomus* | Root vole | Rodentia | 1.000 | 0.000 | 1.000 | 0.001 | 14 | 1.028 |
| Mustela_erminea | *Mustela erminea* | Stoat | Carnivora | 1.334 | 0.334 | 1.334 | 0.117 | 2 | 1.258 |
| Orcinus_orca_2 | *Orcinus orca* | Killer whale | Cetacea | 1.001 | 0.001 | 1.001 | 0.001 | 24 | 0.999 |
| Ovis_aries_2 | *Ovis aries* | Soay sheep | Artiodactyla | 1.033 | 0.033 | 1.033 | 0.020 | 3 | 1.099 |
| Pan_troglodytes_subsp._schweinfurthii | *Pan troglodytes* | Eastern chimpanzee | Primates | 1.000 | 0.000 | 1.000 | 0.001 | 22 | 0.982 |
| Papio_cynocephalus | *Papio cynocephalus* | Olive baboon | Primates | 1.000 | 0.000 | 1.000 | 0.000 | 19 | 1.054 |
| Peromyscus_maniculatus_2 | *Peromyscus maniculatus* | Deer mouse | Rodentia | 1.010 | 0.010 | 1.010 | 0.005 | 2 | 1.107 |
| Phocarctos_hookeri | *Phocarctos hookeri* | New Zealand sea lion | Carnivora | 1.005 | 0.005 | 1.005 | 0.003 | 8 | 1.023 |
| Propithecus_verreauxi | *Propithecus verreauxi* | Verreaux's sifaka | Primates | 1.000 | 0.000 | 1.000 | 0.000 | 12 | 0.986 |
| Puma_concolor_8 | *Puma concolor* | Cougar | Carnivora | NA | NA | NA | NA | 10 | 1.115 |
| Rattus_fuscipes | *Rattus fuscipes* | Bush rat | Rodentia | 1.246 | 0.246 | 1.246 | 0.029 | 2 | 1.305 |
| Spermophilus_armatus | *Urocitellus armatus* | Uinta ground squirrel | Rodentia | 1.016 | 0.016 | 1.016 | 0.011 | 4 | 1.125 |
| Spermophilus_armatus_2 | *Urocitellus armatus* | Uinta ground squirrel | Rodentia | 1.017 | 0.017 | 1.017 | 0.010 | 3 | 1.095 |
| Spermophilus_columbianus | *Urocitellus columbianus* | Columbian ground squirrel | Rodentia | 1.036 | 0.036 | 1.036 | 0.025 | 3 | 1.009 |
| Spermophilus_columbianus_3 | *Urocitellus columbianus* | Columbian ground squirrel | Rodentia | 1.003 | 0.003 | 1.003 | 0.006 | 3 | 1.200 |
| Ursus_americanus_subsp._floridanus | *Ursus americanus* | Florida black bear | Carnivora | 1.003 | 0.003 | 1.003 | 0.003 | 2 | 1.020 |
| Ursus_arctos_subsp._horribilis_5 | *Ursus arctos* | Grizzly bear | Carnivora | 1.001 | 0.001 | 1.001 | 0.001 | 4 | 1.026 |
| Ursus_maritimus_2 | *Ursus maritimus* | Polar bear | Carnivora | 1.019 | 0.019 | 1.019 | 0.007 | 2 | 0.941 |
| Brachyteles_hypoxanthus_2 | *Brachyteles hypoxanthus* | Northern muriqui | Primates | 1.000 | 0.000 | 1.000 | 0.000 | 12 | 1.111 |
| Cebus_capucinus_2 | *Cebus capucinus* | WhiteNAfaced capuchin monkey | Primates | 1.000 | 0.000 | 1.000 | 0.000 | 11 | 1.059 |
| Chlorocebus_aethiops_2 | *Chlorocebus aethiops* | Vervet | Primates | 1.075 | 0.075 | 1.075 | 0.087 | 5 | 1.187 |
| Erythrocebus_patas | *Erythrocebus patas* | Patas monkey | Primates | 1.051 | 0.051 | 1.051 | 0.038 | 5 | 1.128 |
| Gorilla_beringei_subsp._beringei | *Gorilla beringei* | Mountain gorilla | Primates | 1.000 | 0.000 | 1.000 | 0.000 | 21 | 1.053 |

697

698